

Facile one-pot synthesis of Cu-SSZ-39 catalysts with excellent catalytic performance in NH₃-SCR reaction

Jinpeng Du ^{a,b}, Xiaomin Tang ^c, Chi Huang ^{b,e}, Jianqi Liu ^{b,e}, Yulong Shan ^{a,*}, Yan Zhang ^b, Mingsong Ren ^f, Yinhuan Wang ^f, Wenpo Shan ^b, Yunbo Yu ^{a,b,d,e}, Anmin Zheng ^c, Hong He ^{a,b,d,e}

^a State Key Joint Laboratory of Environment Simulation and Pollution Control, Research Center for Eco-Environmental Sciences, Chinese Academy of Sciences, Beijing 100085, China

^b Center for Excellence in Regional Atmospheric Environment, Institute of Urban Environment, Chinese Academy of Sciences, Xiamen 361021, China

^c State Key Laboratory of Magnetic Resonance and Atomic and Molecular Physics, National Center for Magnetic Resonance in Wuhan, Key Laboratory of Magnetic Resonance in Biological Systems, Wuhan Institute of Physics and Mathematics, Innovation Academy for Precision Measurement Science and Technology, Chinese Academy of Sciences, Wuhan 430071, China

^d Ganjiang Innovation Academy, Chinese Academy of Sciences, Ganzhou 341119, China

^e University of Chinese Academy of Sciences, Beijing 100049, China

^f Actblue Co., Ltd., Chizhou 247099, China



ARTICLE INFO

Keywords:

NO_x abatement
NH₃-SCR
Cu-SSZ-39 zeolite
One-pot synthesis
Hydrothermal stability
SO₂ resistance

ABSTRACT

Nitrogen oxide (NO_x) emission from diesel vehicles has caused severe pollution to the atmospheric environment. Selective catalytic reduction of NO_x with NH₃ (NH₃-SCR) technology has been widely used to remove NO_x from diesel vehicle exhaust. Cu-SSZ-39 zeolites have exhibited excellent NH₃-SCR catalytic activity and hydrothermal stability, giving them promise for practical application. A facile one-pot synthesis method to prepare Cu-SSZ-39 zeolites was developed, with complete crystallization achieved in 24 h. Moreover, the Cu content could be controlled by adjusting the amount of Cu-TEPA added without the need for complex post-treatment processes. Cu-SSZ-39 catalysts synthesized through the one-pot synthesis method exhibited excellent NH₃-SCR activity and hydrothermal stability. The one-pot-synthesized Cu-SSZ-39 catalysts contained in situ generated CuO species, which can act as sacrificial sites to protect Cu²⁺ under sulfidation conditions. Considering their efficient synthesis process, excellent NH₃-SCR activity, hydrothermal stability and sulfur resistance, one-pot-synthesized Cu-SSZ-39 catalysts hold great promise for future applications.

1. Introduction

Nitrogen oxide (NO_x) compounds wield substantial influence in the creation of two of the most worrisome air quality concerns: particulate matter (PM) and ozone [1,2]. Notably, NO_x emissions from diesel vehicle exhaust make up a significant portion of these emissions, and disperse widely into the environment [3,4]. Confronting this environmental challenge necessitates innovative solutions, and one technology at the forefront is selective catalytic reduction using ammonia (NH₃-SCR) [5,6]. In the aftertreatment system of diesel vehicle exhaust, a Diesel Particulate Filter (DPF) is placed in front of the SCR system for capturing particulate matter (PM). The DPF requires high-temperature regeneration periodically, which exposes the SCR catalyst to a high-temperature and high-humidity environment. Therefore, both

excellent hydrothermal stability and high NH₃-SCR activity are necessary for SCR catalysts.

Small-pore zeolites are renowned for their exceptional NH₃-SCR catalytic activity and hydrothermal stability, and the Cu-SSZ-13 catalyst has already found practical utility in diesel vehicles. Cu-SSZ-39, which shares structural similarities with Cu-SSZ-13, has also attracted the attention of researchers in recent years [7,8]. A high proportion of Cu²⁺-2Al species and intricate pore structure contribute to its enhanced hydrothermal stability, making it suitable for stringent application conditions [9]. Consequently, an increasing number of studies on Cu-SSZ-39 catalysts have emerged, investigating their resistance to sulfur, alkali metals, alkaline earth metals, and phosphorus, as well as their fast-SCR performance, all of which indicate its potential for practical applications [10–12].

* Corresponding author.

E-mail address: yshan@rcees.ac.cn (Y. Shan).

In conventional approaches for synthesizing Cu-SSZ-39 catalysts, Y zeolite is commonly used as the precursor [13,14]. Afterwards, Xiao et al. developed alternative methods using more cost-effective materials such as Beta zeolite, ZSM-5 zeolite, and conventional silica-alumina sources as precursors for Cu-SSZ-39 synthesis [15,16]. Our team conducted a comparative assessment of Cu-SSZ-39 catalysts derived from these diverse precursors, revealing that those prepared using ZSM-5 as the precursor exhibited superior activity and enhanced hydrothermal stability [17]. The one-pot synthesis method has already been applied to various Cu-based small-pore zeolites, such as Cu-SSZ-13, Cu-SAPO-34, Cu-SSZ-50, and Cu-SSZ-39 [14,18–20]. The one-pot synthesis method offers the advantage of simplifying the synthesis process, making it more amenable to practical-scale production. However, it also presents challenges related to the uncontrollable nature of Cu species and abundant Na^+ ions [21,22]. Corma et al. attempted to use a one-pot synthesis method to prepare Cu-SSZ-39 catalysts; however, due to the lack of control over Cu species, the performance was suboptimal [14]. Hence, there is room for improvement in the one-pot synthesis of Cu-SSZ-39 catalysts to align with the requirements of practical applications.

In this study, an optimized one-pot synthesis method for Cu-SSZ-39 catalysts was developed, utilizing *N,N*-diethyl-cis-2,6-dimethylpiperidinium hydroxide (DEDMPOH) and Cu-tetraethylenepentamine (Cu-TEPA) as co-templating agents. Using ZSM-5 zeolites as precursors, the synthesized Cu-SSZ-39 zeolites present excellent catalytic performance, moreover, the price of ZSM-5 is also cheaper than Y. Therefore, ZSM-5 zeolites were utilized as the precursors in this study. First, we confirmed the feasibility of synthesizing Cu-SSZ-39 by one-pot method thorough theoretical calculations. Control over the Cu content in the Cu-SSZ-39 catalysts was achieved by adjusting the amount of Cu-TEPA added, eliminating the need for a complex post-treatment process. The crystallization process of the Cu-SSZ-39 catalysts was explored through XRD and SEM. The morphology, structure, and copper species of the catalysts were investigated using XRD, SEM NMR, TGA/DSC, H_2 -TPR, EPR, NH_3 -TPD and DRIFTS. The catalytic performance of the Cu-SSZ-39 catalysts prepared by the one-pot synthesis method was compared to that of commercially available Cu-SSZ-13 catalysts. Furthermore, the sulfur resistance of catalysts prepared through the one-pot synthesis and ion-exchange methods was evaluated. A thorough investigation encompassing the crystallization process, catalyst properties and catalytic performance was carried out, establishing a robust foundation for practical application.

2. Experimental

2.1. Catalyst preparation

Cu-SSZ-39 catalysts were prepared by employing DEDMPOH and Cu-TEPA as co-templates along with ZSM-5 (Si/Al~12) as precursors. The detailed preparation process is illustrated in the [supporting information](#). The obtained catalysts were named: $\text{Cu}_{0.3}$ -SSZ-39-OP, $\text{Cu}_{0.8}$ -SSZ-39-OP, $\text{Cu}_{1.5}$ -SSZ-39-OP, and $\text{Cu}_{2.3}$ -SSZ-39-OP according to the results of ICP-OES. For comparison, an ion-exchanged Cu-SSZ-39 sample was obtained with ZSM-5 as precursor and designated as $\text{Cu}_{2.0}$ -SSZ-39-IE.

2.2. Theoretical calculation

Stabilization energy, which was defined as the difference between the energy of the zeolite-template complex with the energy of templates and empty zeolite framework, was used to evaluate the feasibility of transformation from MFI to AEI framework in the presence of co-templating agents, namely Cu-TEPA and DEDMP in this work. The MFI and AEI frameworks were obtained from the IZA database [23] and treated as neutral pure silica frameworks. The zeolite frameworks (MFI and AEI), co-templating agents (Cu-TEPA and DEDMP), as well as their complexes were firstly optimized under the constant volume condition and then performed molecular dynamics (MD) simulations using the

universal force field (UFF) [24] taking advantage of the General Utility Lattice Program (GULP) package [25]. The reported energy values were taken as the average energy calculated from the last 5 ps of a 30 ps MD simulation with a timestep of 0.5 fs at 413 K (the synthesis temperature) in the NVT ensemble. On the basis of the average energy results for 10,000 possible configurations under synthetic conditions in the MD calculation, the stabilization energy was calculated as the following equation:

$$\text{Stabilization energy} = [E(\text{zeolite}_n \text{ template}) - E(\text{zeolite}) - n_1 E(\text{template-1}) - n_2 E(\text{template-2})]/NT$$

The $E(\text{zeolite}_n \text{ template})$, $E(\text{zeolite})$, $E(\text{template-1})$ and $E(\text{template-2})$ were the energies of the zeolite-template complex, empty MFI or AEI framework, isolated Cu-TEPA and isolated DEDMP, respectively. n was the total number of templates in zeolite framework and was the sum of n_1 and n_2 , where n_1 and n_2 were the number of template-1 (i.e., Cu-TEPA) and template-2 (i.e., DEDMP), with n , n_1 and n_2 equal to 4, 2, and 2, respectively (detailed reason was explained in the [supporting information](#)). NT was the number of T atoms in zeolite framework, which was 96 for MFI framework while 48 for AEI framework.

2.3. Characterization

The elemental compositions of the catalysts were assessed via inductively coupled plasma optical emission spectrometry (ICP-OES) using a PerkinElmer Optima 8300 spectrometer. The catalysts' crystallization was investigated using X-ray diffraction (XRD) on a Brucker D8 Advance diffractometer, which employed Cu $\text{K}\alpha$ as radiation source ($\lambda = 0.15406 \text{ nm}$). Analysis of catalyst morphology was performed using scanning electron microscopy (SEM) with a Hitachi S4800 microscope. Raman was used to investigate the crystallization process of one-pot synthesized Cu-SSZ-39 catalysts. Experiments were carried out on Renishaw (inVia) with the wavenumber of light source of 532 nm. Utilizing a Bruker 600 M spectrometer, nuclear magnetic resonance (NMR) was employed to investigate the coordination environment of framework atoms. Catalyst weight changes and heat absorption/loss as a function of temperature were monitored using Thermal Gravimetric Analysis (TGA) and Differential Scanning Calorimetry (DSC) on a Mettler Toledo device (TGA/DSC 1 Star E System). The experiments were conducted with air as the carrier gas, a constant gas flow rate of 50 mL/min, and a temperature ramp rate of 10 °C/min.

The Cu-SSZ-39 catalysts' redox capacity was evaluated through hydrogen temperature programmed reduction (H_2 -TPR) experiments, which were performed on a Micromeritics AutoChem 2920 chemisorption analyzer, and electron paramagnetic resonance (EPR) experiments were performed at 120 K using a Bruker E500 EPR spectrometer to analyze the paramagnetic Cu ions. *In situ* Diffuse Reflectance Infrared Fourier Transform Spectroscopy (DRIFTS) was employed to identify Cu species within the catalysts. Ammonia temperature programmed desorption (NH_3 -TPD) experiments were conducted to evaluate the catalysts' acidity. Detailed descriptions of H_2 -TPR, *in situ* DRIFTS and NH_3 -TPD experiments are provided in the [supporting information](#). Sulfated species were distinguished by SO_2 -TPD experiments, where the exhaust gas was detected using mass spectrometry (Hiden Analytical HPR-20 EGA).

2.4. NH_3 -SCR catalytic activity test

NH_3 -SCR tests were carried out to evaluate the catalytic performance of prepared catalysts. The inlet gas mixture comprised 500 ppm NO, 500 ppm NH_3 , 5 % O_2 , 5 % H_2O , and N_2 as balance gas. The overall gas flow rate was 500 mL/min, and the gas hourly space velocity (GHSV) was 200,000 h^{-1} . The outlet gas composition was analyzed using an online infrared spectrometer (Thermo Nicolet IS50). NO_x conversion was determined using the following equation:

$$NO_x\text{conversion} = \left(1 - \frac{[NO_x]_{\text{out}}}{[NO_x]_{\text{in}}}\right) \times 100\% \quad (\text{NO}_x = \text{NO} + \text{NO}_2)$$

To evaluate the hydrothermal stability and sulfur resistance of the prepared catalysts, hydrothermal aging and sulfidation treatments were carried out, and the detailed experimental procedures are illustrated in the [supporting information](#). The obtained hydrothermally aged catalysts were named: $\text{Cu}_{0.3}\text{-SSZ-39-OP HTA}$, $\text{Cu}_{0.8}\text{-SSZ-39-OP HTA}$, $\text{Cu}_{1.5}\text{-SSZ-39-OP HTA}$, and $\text{Cu}_{2.3}\text{-SSZ-39-OP HTA}$, respectively. The sulfidation and regeneration catalysts were named: $\text{Cu}_{2.3}\text{-SSZ-39-OP-S}$, $\text{Cu}_{2.0}\text{-SSZ-39-IE-S}$, $\text{Cu}_{2.3}\text{-SSZ-39-OP-S-R}$ and $\text{Cu}_{2.0}\text{-SSZ-39-IE-S-R}$. A commercial Cu -SSZ-13 catalyst named Cu -SSZ-13-commercial was also used to compare its $\text{NH}_3\text{-SCR}$ activity with that of $\text{Cu}_{2.3}\text{-SSZ-39-OP}$.

3. Results

3.1. Properties of one-pot-synthesized Cu -SSZ-39 catalysts

3.1.1. Crystallization process prediction and characterization

Theoretical calculation is useful for assessing the feasibility of templates for synthesizing zeolites [26–29], which would improve the efficiency for screening templates. Therefore, the theoretical calculation was performed before synthesis process. In this work, the stabilization energy was used as a parameter to estimate the contribution of co-templating agents (*i.e.*, Cu-TEPA and DEDMP) on transformation from ZSM-5 zeolite (MFI topology) to SSZ-39 zeolite (AEI topology). The optimized typical positions of co-templating agents in zeolites were presented in [Fig. 1](#). As presented in [Table 1](#), the stabilization energy with the co-existence of Cu-TEPA and DEDMP in MFI (-3.87 kJ/mol-Si) was much weaker than that in AEI (-14.54 kJ/mol-Si), suggesting the possibility of conversion from MFI to AEI framework in the presence of co-templating agents. Encouraged by theoretical results, the Cu-SSZ-39 catalyst was successfully synthesized by the one-pot method. Therefore, the calculation in this work theoretically demonstrated that the co-templating agents could not only promote the transformation from MFI to AEI framework, but also introduce Cu^{2+} into SSZ-39 zeolite, which eliminated the need for complicated post-treatment process and provided insights into the one-pot synthesis of copper-containing catalysts.

To investigate the crystallization process of the catalyst, XRD and SEM experiments were carried out for the catalysts crystallized for 12 h, 24 h, 48 h, 72 h, 96 h and 120 h. In order to ensure consistency, the amount of CuSO_4 and TEPA added in the preparation of all catalysts was equal to that used in $\text{Cu}_{2.3}\text{-SSZ-39-OP}$. As presented in [Fig. 2 \(a\)](#), the profile at 0 h corresponded to the diffraction peaks of the precursor

Table 1
Calculated stabilization energy of OSDA-zeolite.

Zeolite framework	MFI	AEI
Stability energy, OSDA-zeolite (kJ/mol Si)	-3.87	-14.54

ZSM-5 zeolite. After crystallizing for 12 h, the intensity of the ZSM-5 diffraction peaks decreased significantly, and the diffraction peaks of SSZ-39 zeolite emerged. After crystallizing for 24 h, all ZSM-5 diffraction peaks disappeared, and the catalyst exhibited the diffraction peaks of SSZ-39 only. We calculated the relative peak intensities with 20 of 17.7°, 20.7°, 21.4°, 24.1° and 31.3° to investigate the relationship between crystallization time and crystallinity [30,31]. As presented in [Fig. 2 \(b\)](#), little change in the relative crystallinity can be observed from 24 h to 120 h, indicating that this catalyst can be fully crystallized in 24 h.

Morphological changes of the catalysts during the crystallization process were also investigated through SEM, and the results are summarized in [Figure S1](#). From [Figure S1\(a-b\)](#), it can be observed that the precursor ZSM-5 zeolite exhibited a smooth-surfaced cubic structure. As shown in [Figure S1\(c-d\)](#), after 12 h of crystallization, a mesoporous structure appeared during the dissociation of the ZSM-5 zeolite. The ZSM-5 zeolite gradually broke down into small particles, accompanied by the appearance of some irregular spherical particles. These irregular spherical particles with diameter $\sim 1\text{ }\mu\text{m}$ dominated after crystallization for 24 h, as presented in [Figure S1\(e-f\)](#). Moreover, little change can be observed in the morphology of the catalysts between 24 h and 120 h of crystallization, as shown in [Figure S1\(e-h\)](#). This indicates that $\sim 100\%$ crystallinity can be achieved for the one-pot synthesized Cu-SSZ-39 catalyst in 24 h, in accordance with the XRD results.

The Raman spectroscopy was further employed to investigate the crystallization process of one-pot synthesized Cu-SSZ-39 zeolites, as depicted in [Fig. 2 \(c\)](#). The peak at 294 cm^{-1} corresponded to the S6R unit in ZSM-5 zeolite, while peaks at 302 cm^{-1} and 334 cm^{-1} were attributed to the D6R unit in SSZ-39 zeolite [32]. The peak intensity of the S6R in ZSM-5 gradually decreased during 2–4 h, and no signal of D6R in SSZ-39 was observed simultaneously. This indicated that the S6R unit in ZSM-5 decomposed first during the crystallization process. Meanwhile, the signal of D6R in SSZ-39 emerged from the 6th hour. The peak at 380 cm^{-1} was assigned to the S5R unit in ZSM-5 zeolite [32], and this unit diminished continuously until completely disappeared after 12 h. The peak at 453 cm^{-1} was attributed to the S4R unit in ZSM-5, while peaks at 466 cm^{-1} and 481 cm^{-1} corresponded to the S4R unit in SSZ-39 zeolite [32,33]. The S4R unit in SSZ-39 was observed in 2–4 h with a reduction in the S4R unit in ZSM-5. This indicated the

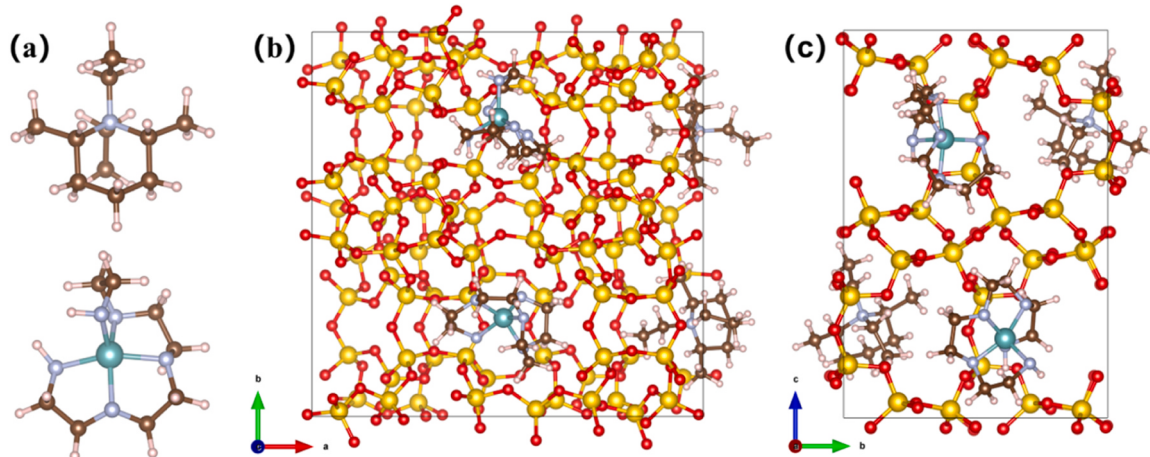


Fig. 1. (a) Configurations of co-templating agents, the top and bottom are DEDMP and Cu-TEPA, respectively. Optimized positions of co-templating agents (*i.e.*, Cu-TEPA and DEDMP) in (a) MFI and (b) AEI zeolite framework. Color code: Si, yellow; O, red; C, brown; H, bare; Cu, cyan; N, light blue.

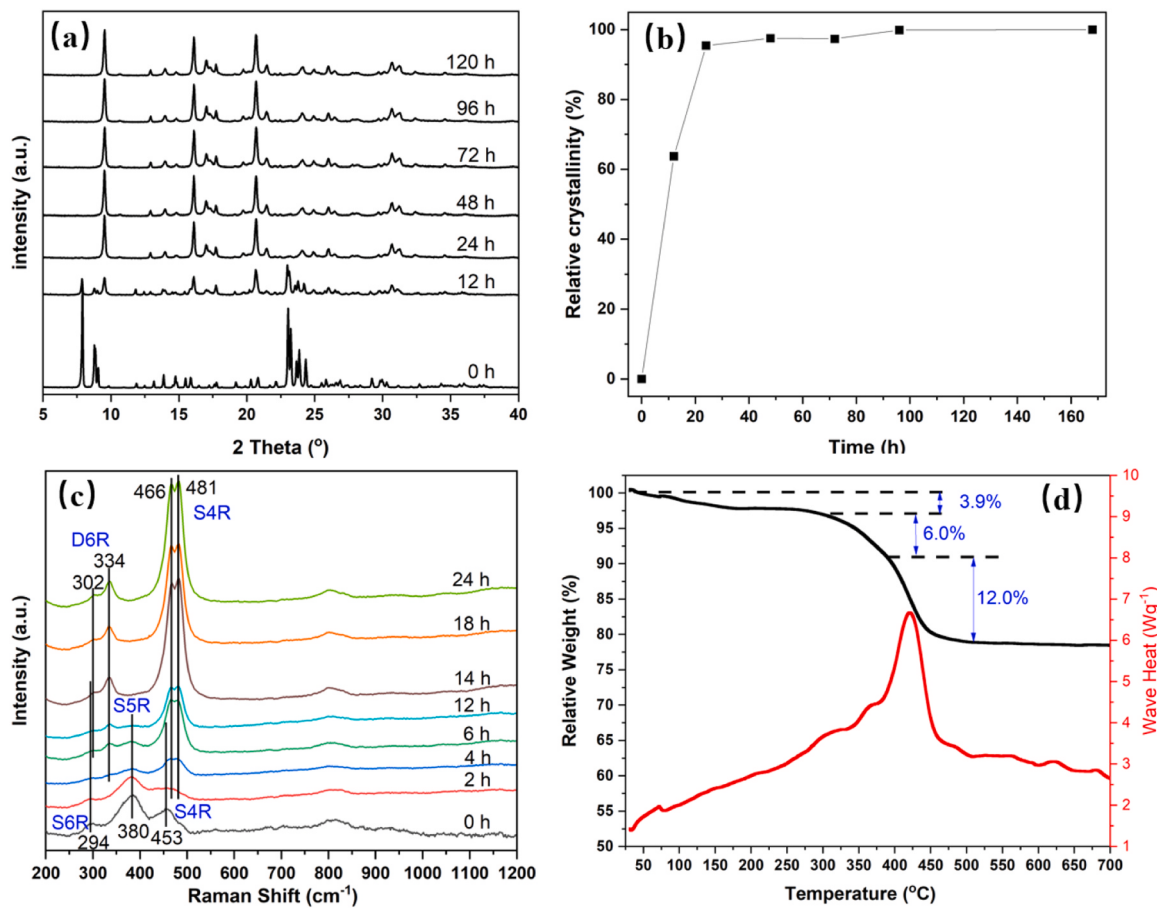


Fig. 2. (a) XRD profiles and (b) Relative crystallinity of one-pot-synthesized Cu-SSZ-39 catalysts after crystallization for 0 h, 12 h, 24 h, 48 h, 72 h, 96 h and 120 h; (c) Raman spectra of one-pot-synthesized Cu-SSZ-39 catalysts after crystallization for 0 h, 2 h, 4 h, 6 h, 12 h, 14 h, 18 h and 24 h; (d) TGA-DSC curve of one-pot-synthesized Cu-SSZ-39 catalysts after crystallization for 96 h.

direct transformation of the S4R unit in ZSM-5 into the S4R unit in SSZ-39. In summary, during the crystallization process, the S6R and S5R units in ZSM-5 decomposed, while the S4R unit transformed directly into the S4R unit in SSZ-39, forming the D6R unit. This process aligned with the studies of Xiao et al., when investigating the transformation of ZSM-5 zeolite into SSZ-39 zeolite [32]. It indicated that the addition of Cu-TEPA did not influence the crystallization process of SSZ-39 prepared by ZSM-5.

To investigate the changes in mass and thermal signals of samples during the heating process, a catalyst with crystallization time of 96 h was chosen for a TG-DSC experiment. As presented in Fig. 2 (d), the mass of the catalyst decreased gradually by ~3.9 % from 25°C to 300°C, which was primarily attributed to the evaporation of moisture. Between 300 and 450°C, there was a rapid decrease in the catalyst's mass, accompanied by fluctuations in the thermal signal. According to previous studies, the weight loss around 300–380°C was due to the decomposition of TEPA, and constituted 6 % of the sample's total mass [34]. The further decrease in weight from 380°C to 450°C was due to the combustion of DEDMPOH, which accounted for 12 % of the weight of the catalyst [15].

3.1.2. Physical properties of one-pot-synthesized Cu-SSZ-39 catalysts

Fig. 3 (a) shows the XRD patterns of one-pot-synthesized Cu-SSZ-39 catalysts with different Cu contents. It can be observed that all catalysts exhibited characteristic diffraction peaks of the AEI structure. With the increase in Cu content, the intensity of the diffraction peaks of the catalysts decreased, indicating that the addition of Cu-TEPA affected the crystallinity of one-pot-synthesized Cu-SSZ-39 catalysts. However, no

diffraction peaks corresponding to CuO were observed in the patterns of any of the catalysts. Table 2 lists the elemental contents of different catalysts. It can be seen that with the increase in the amount of Cu-TEPA added to the starting gel, the Cu content in the products also rose. Meanwhile, with an increase in the Cu Content, the Si/Al ratio of the catalysts presented a decreasing trend. During the synthesis process of zeolites, templates with positive charge needs Al atoms in the framework to compensate the charge. Each Cu-TEPA molecules contain two positive charges, and each DEDMP molecule contains one positive charge. When more Cu-TEPA molecules existed, more framework Al atoms were produced, resulting in lower Si/Al ratio. The same phenomenon was also observed in our previous research on one-pot synthesis of Cu-SSZ-50 zeolites [19]. It is worth noting that due to the absence of a post-treatment process, the one-pot-synthesized Cu-SSZ-39 catalysts still contain 0.3–0.5 wt% of Na⁺. The effect of Na⁺ will be discussed in the following sections.

Fig. 3 (b-e) displays SEM images of one-pot-synthesized Cu-SSZ-39 catalysts with different Cu contents. It can be observed that Cu_{0.3}-SSZ-39-OP exhibited a cubic morphology with particle size around 1 μm, which is similar to the Cu-SSZ-39 catalyst prepared using ZSM-5 as a precursor via the ion exchange method [17]. When the Cu content increased to 0.8 %, the cubic structure was still maintained, but the particle size decreased to around 300–500 nm. This is because that both Cu-TEPA and DEDMP molecules acted as structure directing agents. When more Cu-TEPA molecules were introduced, they accelerated the nucleation of zeolites, which resulted in smaller particle size. With the further increase of Cu-TEPA, the nucleation process was further accelerated, and even smaller particles were formed. However, these smaller

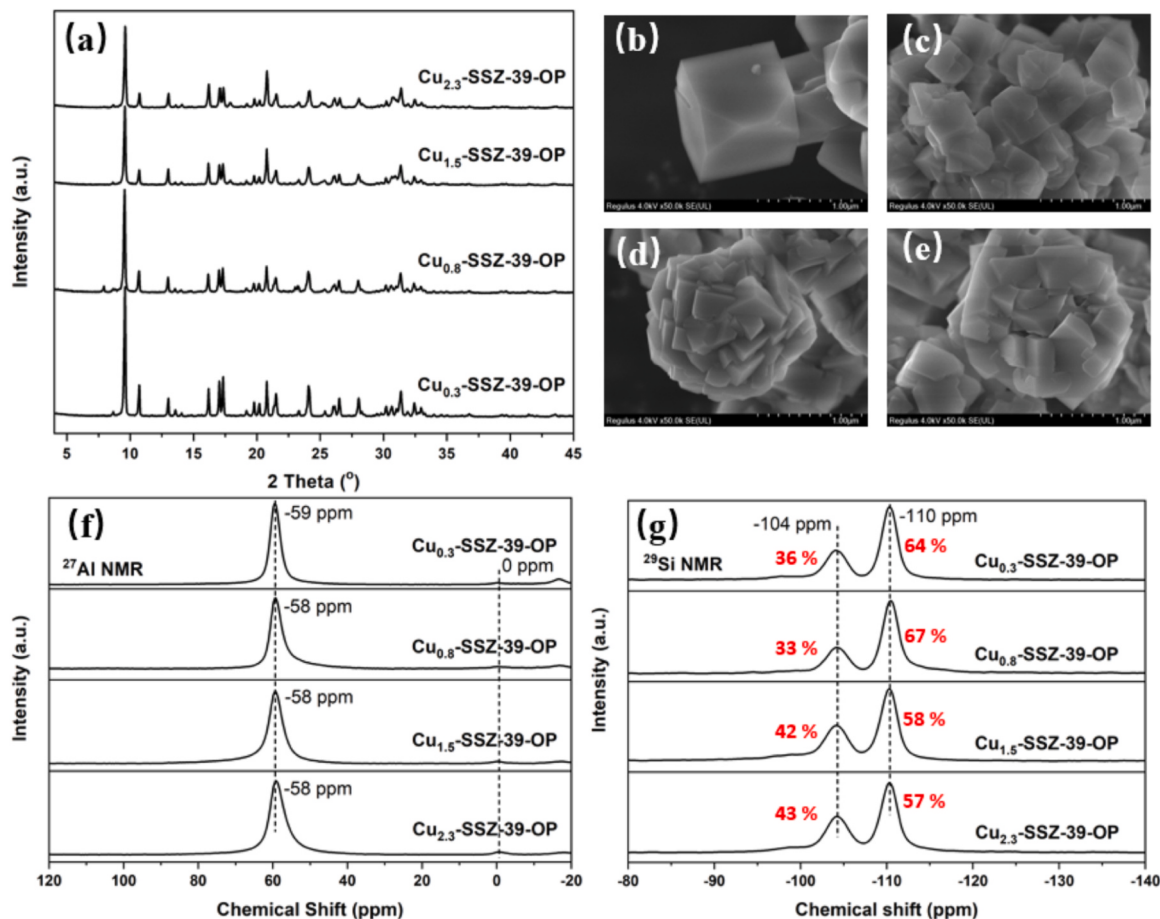


Fig. 3. (a) XRD patterns, (b-e) SEM images, (f) ²⁷Al NMR and (g) ²⁹Si NMR of one-pot-synthesized Cu-SSZ-39 catalysts with various Cu contents.

Table 2

Elemental composition of one-pot synthesized Cu-SSZ-39 catalysts, ion-exchanged Cu-SSZ-39 catalyst and commercial Cu-SSZ-13 catalyst.

Samples	Cu	Si	Al	Na	Cu/Al	Si/Al
Cu _{0.3} -SSZ-39-OP	0.3	29.1	3.1	0.4	0.04	8.9
Cu _{0.8} -SSZ-39-OP	0.8	30.4	3.3	0.3	0.10	8.9
Cu _{1.5} -SSZ-39-OP	1.5	29.8	3.9	0.5	0.16	7.4
Cu _{2.3} -SSZ-39-OP	2.3	28.6	4.2	0.5	0.23	6.6
Cu _{2.0} -SSZ-39-IE	2.0	34.2	3.7	0	0.23	8.9
Cu-SSZ-13 commercial	2.1	28.6	4.2	0.02	0.21	6.6

particles grew together, so the morphology of Cu_{1.5}-SSZ-39-OP and Cu_{2.3}-SSZ-39-OP presented the 'flower-like' structure. This suggested that further increasing the Cu-TEPA content can significantly affect the crystallization of one-pot-synthesized Cu-SSZ-39 catalysts, consistent with the XRD results.

TEM and EDS-mapping images of the one-pot-synthesized Cu-SSZ-39 catalysts are presented in Figure S2. The morphology of the complete catalyst particles has been presented in the SEM images, therefore, we chose to magnify the specific local regions in the TEM images. It can be observed that the cubic structure of the catalysts with four different Cu contents is visible after the local magnification, consistent with our SEM analysis. Moreover, it can be observed that Cu, Si, and Al are uniformly distributed within all catalysts as shown in the EDS mapping images. This indicates that one-pot-synthesis method does not result in uneven distribution of elements within the zeolites, which provides assurance for excellent catalytic activity.

Fig. 3 (f-g) presents the ²⁷Al and ²⁹Si NMR spectra of different catalysts, respectively. In the ²⁷Al NMR spectrum, the peak at \sim 58 ppm

represents tetrahedrally coordinated framework Al, while the peak at \sim 0 ppm corresponds to hexahedrally coordinated extra-framework Al [35,36]. It can be observed that there was no significant presence of extra-framework Al in the one-pot-synthesized Cu-SSZ-39 catalysts with various Cu contents, indicating that all the catalysts' framework structures were well-crystallized. In the ²⁹Si NMR spectrum, the peaks at \sim 110 ppm and \sim 104 ppm were attributed to Si (4Si0Al) species and Si (3Si1Al) species, respectively [7,35]. It can be seen that compared with Cu_{0.3}-SSZ-39-OP and Cu_{0.8}-SSZ-39-OP, the higher-loaded samples contained a higher proportion of Si species (3Si1Al). This indicated the presence of higher amounts of framework Al atoms in Cu_{1.5}-SSZ-39-OP and Cu_{2.3}-SSZ-39-OP, which aligned with the ICP results. Overall, the Si and Al atoms were well-arranged in all of the catalysts with different Cu contents, which was beneficial for the stability of Cu species.

3.1.3. Cu species and acid sites of one-pot-synthesized Cu-SSZ-39 catalysts

EPR was used to investigate the coordination environment and quantity of divalent Cu ions in one-pot-synthesized Cu-SSZ-39 catalysts, and the spectra are shown in Fig. 4 (a). All Cu-SSZ-39 catalysts presented EPR spectra characterized by a fourfold hyperfine splitting pattern with a single g ($g_{\text{II}} = 2.39$, $A_{\text{II}} = 134$ G), which was assigned to Cu²⁺ or Cu (OH)⁺ species [37,38]. The EPR signal of one-pot-synthesized Cu-SSZ-39 catalysts was elevated with the increase in Cu loading, indicating that more divalent ions existed. In order to distinguish between Cu²⁺ and Cu (OH)⁺ species in one-pot-synthesized Cu-SSZ-39 catalysts, *in situ* DRIFTS of NH₃ adsorption experiments were conducted with results shown in Fig. 4 (b). Since NH₃ changes the coordination environment of Cu ions with framework atoms after complexation, peaks in the wavenumber range of 900–950 cm⁻¹ can be used to differentiate Cu ions with different coordination states [39,40]. In Cu-SSZ-39 catalysts, the peak at

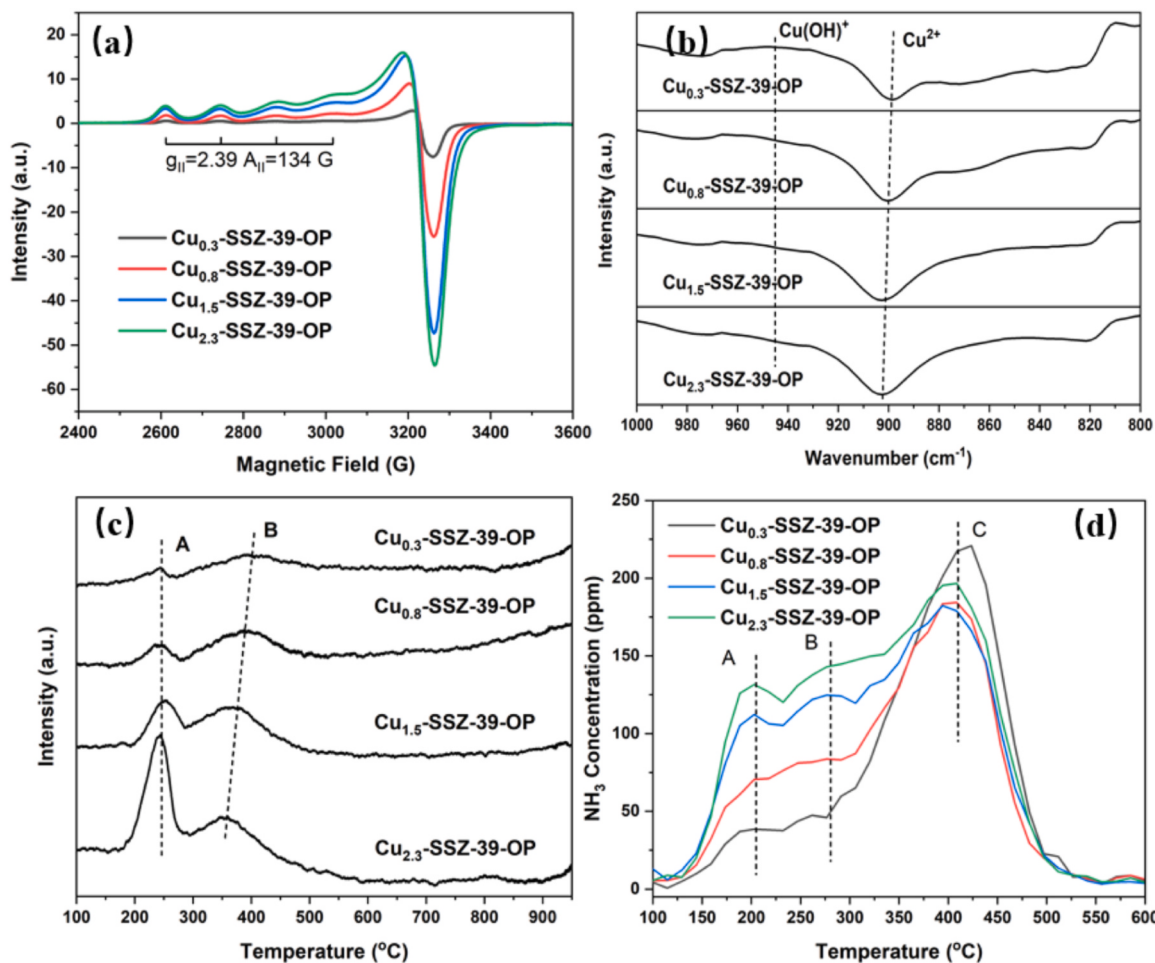


Fig. 4. (a) EPR spectra, (b) *in situ* DRIFTS of NH₃ adsorption spectra, (c) H₂-TPR profiles and (d) NH₃-TPD profiles of one-pot-synthesized Cu-SSZ-39 catalysts with various Cu contents.

around 940 cm⁻¹ is attributed to Cu(OH)⁺ species, while the peak at around 900 cm⁻¹ is attributed to Cu²⁺ species [9,17]. It can be observed that in one-pot-synthesized Cu-SSZ-39 catalysts with various Cu contents, Cu species primarily existed in the form of Cu²⁺, and Cu(OH)⁺ species were virtually absent.

To further investigate whether other forms of Cu species existed in the one-pot-synthesized Cu-SSZ-39 catalysts, H₂-TPR experiments were conducted. The results showed (Fig. 4 (c)) that two H₂ reduction peaks were observed for all tested catalysts, with peak A attributed to CuO species and peak B attributed to Cu²⁺ species [9,41]. No reduction peak corresponding to Cu(OH)⁺ species was observed, which is consistent with the results of *in situ* DRIFTS experiments. As we mentioned in the discussion on ICP results, one-pot-synthesized Cu-SSZ-39 samples with different Cu contents all contained a certain amount of Na⁺ ions. Na⁺ ions can occupy ion-exchange sites, which causes an insufficiency of ion-exchange sites for Cu ions, leading to the formation of CuO species [18,42]. These CuO species may affect the catalytic performance of catalysts, which will be further explored in the following sections.

Subsequently, we further investigated the acid sites of the catalysts through NH₃-TPD, and the results are shown in Fig. 4(d). In all catalysts, peak A was attributed to weak acid sites, primarily originating from terminal hydroxyl groups; peak B was assigned to moderate acid sites, mainly associated with Lewis acid sites (Cu²⁺); peak C was identified as arising from strong acid sites, primarily attributed to Brønsted acid sites [43,44]. It can be observed that Brønsted acid sites dominated in Cu_{0.3}-SSZ-39-OP and Cu_{0.8}-SSZ-39-OP. With increasing Cu content, both weak acid sites and moderate acid sites increased in number. This is due

to the lower Si/Al ratio leading to an increase in the amount of terminal hydroxyl groups, and the increase in Cu²⁺ species resulted in the formation of more Lewis acid sites.

3.2. Catalytic performance, hydrothermal stability and SO₂ resistance

3.2.1. Catalytic performance and hydrothermal stability of one-pot-synthesized Cu-SSZ-39 catalysts

Fig. 5 presents the NH₃-SCR performance of fresh and hydrothermally aged one-pot-synthesized Cu-SSZ-39 catalysts. As can be seen in Fig. 5 (a), the NO_x conversion of one-pot-synthesized Cu-SSZ-39 catalysts increased with Cu content below 400°C. This was attributed to the increase in the number of SCR-active Cu²⁺ species as well as Lewis acid sites, as illustrated by the EPR and NH₃-TPD results. However, Cu_{2.3}-SSZ-39-OP exhibited lower catalytic activity at higher temperatures (above 500°C), compared with other samples with lower Cu content. This is because Cu_{2.3}-SSZ-39-OP contained a significant amount of CuO species, as indicated by the H₂-TPR results, resulting in NH₃ oxidation at high temperatures. It is worth noting that even though CuO species also existed in Cu_{0.3}-SSZ-39-OP, Cu_{0.8}-SSZ-39-OP, and Cu_{1.5}-SSZ-39-OP, there was no observed decline in high-temperature catalytic activity.

As shown in Fig. 5(b), catalysts with different Cu contents exhibited a decline in catalytic activity after hydrothermal aging at 850°C for 16 h. Nevertheless, Cu_{2.3}-SSZ-39-OP-HTA still maintained NO_x conversion over 88 % in the temperature range of 225–500°C. Cu_{2.3}-SSZ-39-OP-HTA possessed comparable catalytic performance to the Cu-SSZ-39 catalysts prepared using ion-exchange methods with ZSM-5 as a

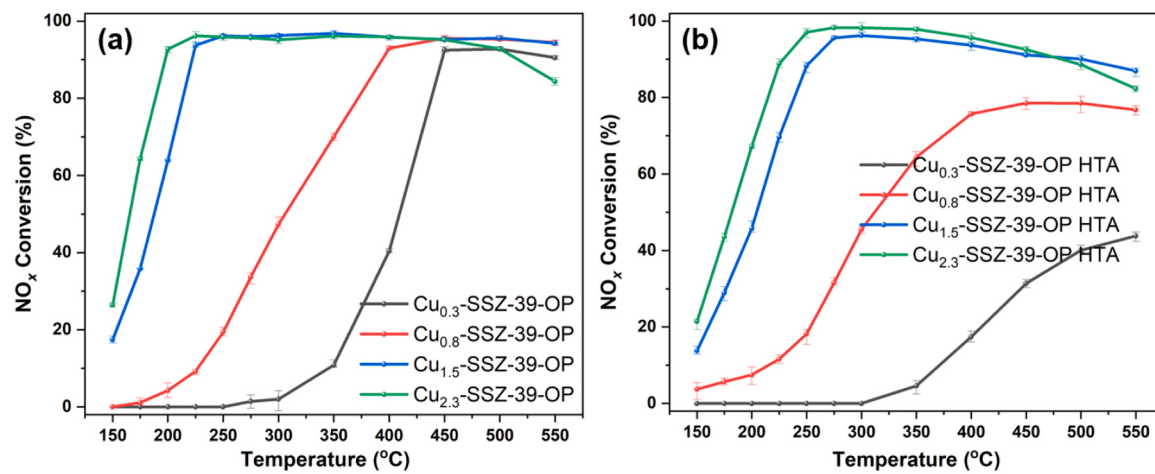


Fig. 5. NH₃-SCR performance of: (a) fresh one-pot-synthesized Cu-SSZ-39 catalysts; (b) aged one-pot-synthesized Cu-SSZ-39 catalysts.

precursor, as previously reported [17]. The NH₃-SCR results illustrated that even though Cu_{2.3}-SSZ-39-OP contained some Na⁺ ions and CuO species, it still possessed excellent NH₃-SCR activity and hydrothermal stability.

Furthermore, N₂O concentration of the fresh and aged one-pot-synthesized Cu-SSZ-39 catalysts during NH₃-SCR tests was summarized in Figure S3. The N₂O concentration of all prepared fresh catalysts was lower than 3 ppm in the whole temperature range, indicating the fresh catalysts possessed excellent N₂ selectivity. In the hydrothermally

aged catalysts, higher amount of N₂O was produced, especially in the Cu_{2.3}-SSZ-39-OP-HTA sample. Nevertheless, no more than 9 ppm of N₂O was produced in the whole temperature range in Cu_{2.3}-SSZ-39-OP-HTA, which was much lower than the N₂O produced by Cu-SSZ-13 as reported by Yao et al. [45,46]. Therefore, we can conclude that the one-pot-synthesized Cu-SSZ-39 catalysts presented excellent N₂ selectivity, and limited N₂O was formed during NH₃-SCR tests.

Fig. 6 (a) presents the XRD patterns of the hydrothermally aged one-pot-synthesized Cu-SSZ-39 catalysts with different Cu loadings. It can be

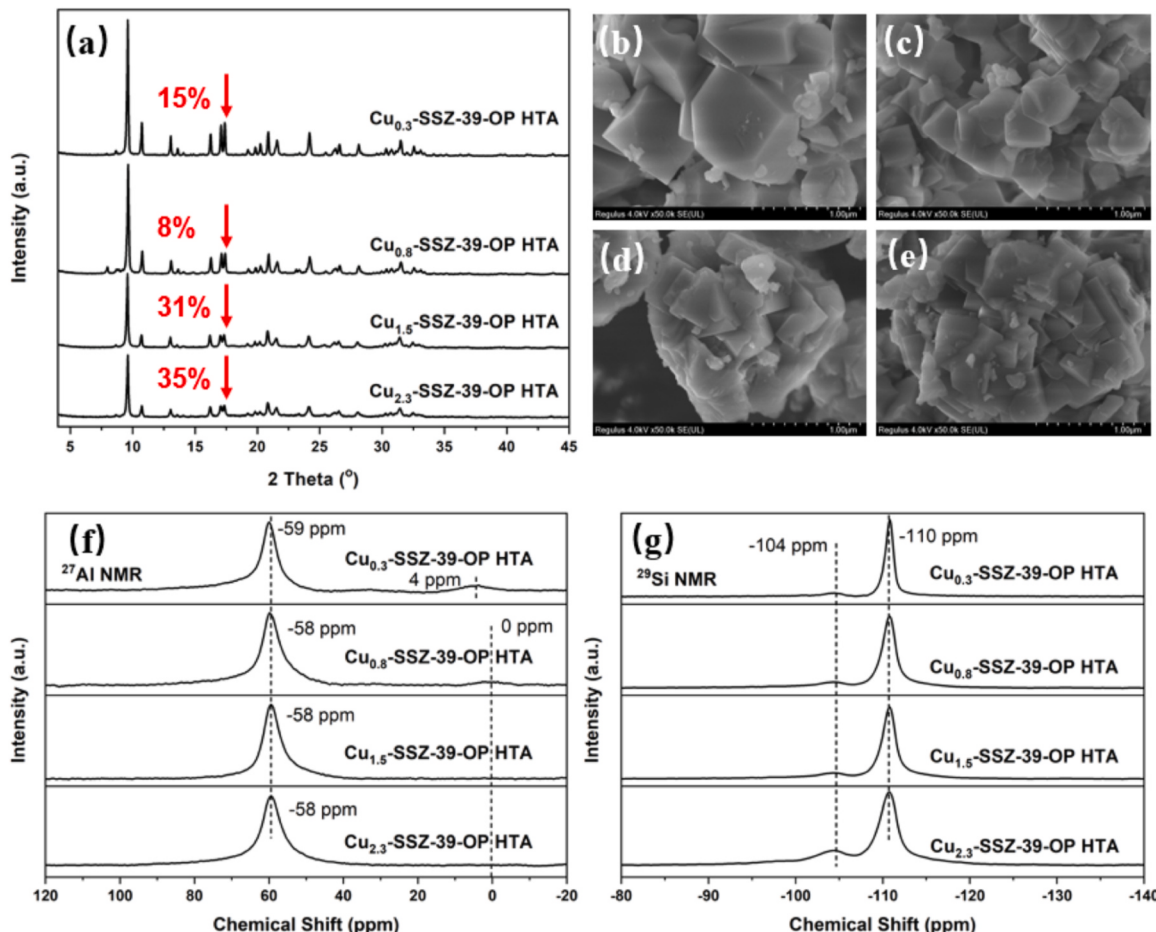


Fig. 6. (a) XRD patterns, (b-e) SEM images, (f) ²⁷Al NMR and (g) ²⁹Si NMR of hydrothermally aged one-pot-synthesized Cu-SSZ-39 catalysts with various Cu contents.

seen that all the catalysts still retained the complete set of AEI diffraction peaks with good crystallinity. In order to compare the crystallinity of fresh and aged one-pot-synthesized Cu-SSZ-39 catalysts, the intensities of peaks with 20 of 17.7°, 20.7°, 21.4°, 24.1° and 31.3° were calculated [30,31]. It was found that the relative crystallinity of $\text{Cu}_{0.3}\text{-SSZ-39-OP}$ and $\text{Cu}_{0.8}\text{-SSZ-39-OP}$ only decreased by 15 % and 8 %, respectively. However, the relative crystallinity of two one-pot-synthesized Cu-SSZ-39 catalysts with high Cu loading decreased by more than 30 %. The $\text{H}_2\text{-TPR}$ results showed that $\text{Cu}_{1.5}\text{-SSZ-39-OP}$ and $\text{Cu}_{2.3}\text{-SSZ-39-OP}$ possessed large amounts of CuO species. The migration of CuO species during the hydrothermal aging process accelerated the damage to the framework, thus causing the relative crystallinity to decrease remarkably.

Fig. 6 (b-e) shows the SEM images of one-pot-synthesized Cu-SSZ-39 catalysts. The hydrothermally aged one-pot-synthesized Cu-SSZ-39 catalysts exhibited similar morphologies to those of the fresh samples, but some small particles were also generated. This phenomenon indicated that the hydrothermal aging process had limited impact on the morphology of the catalysts.

Fig. 6 (f-g) presents the ^{27}Al NMR and ^{29}Si NMR spectra of the hydrothermally aged one-pot-synthesized Cu-SSZ-39 catalysts with different Cu contents. The peak assignments are the same as those in Fig. 3 (f-g). It can be seen that except for the weak peak at 4 ppm in $\text{Cu}_{0.3}\text{-SSZ-39-OP-HTA}$, there was almost no peak observed near 0 ppm for the other catalysts. From the ^{29}Si NMR spectrum, it can be seen that compared with the fresh catalysts, the peak proportion at -104 ppm in all one-pot-synthesized Cu-SSZ-39 catalysts decreased, indicating that dealumination occurred. Combined with the results presented in Fig. 6

(a) showing that the crystallinity of the hydrothermally aged catalysts declined, it can be inferred that dealumination occurred. The lack of a non-framework Al peak in the ^{27}Al NMR spectrum was probably due to the paramagnetic effect of Cu, which shielded the signal of extra-framework Al [47,48].

As shown in Fig. 7 (a), after hydrothermal aging, one-pot-synthesized Cu-SSZ-39 catalysts with various Cu contents still exhibited a fourfold hyperfine splitting pattern with $g_{\parallel}=2.39$, $A_{\parallel}=136$ G, similar to the fresh samples. This demonstrated that the hydrothermal aging process did not produce CuAlO_x species [49]. To compare the contents of divalent Cu ions in the fresh and aged one-pot-synthesized Cu-SSZ-39 catalysts, we calculated the relative Cu contents of samples via double integration of the EPR signals. As shown in Figure S4, with increasing Cu content, the amount of divalent Cu ions increased in both fresh and aged samples. However, compared with the fresh catalysts, all hydrothermally aged catalysts presented a decrease in the number of divalent Cu ions. This indicated that hydrothermal aging led to the loss of Cu^{2+} species.

An *in situ* DRIFTS of NH_3 adsorption experiment was used to differentiate the types of Cu ions in the hydrothermally aged one-pot-synthesized Cu-SSZ-39 catalysts. As shown in Fig. 7 (b), Cu ions still primarily existed in the form of Cu^{2+} in the hydrothermally aged catalysts, which was consistent with the fresh samples. Fig. 7 (c) presents the $\text{H}_2\text{-TPR}$ profiles of the hydrothermally aged one-pot-synthesized Cu-SSZ-39 catalysts. Peaks A and B were attributed to the H_2 reduction of CuO and Cu^{2+} species, respectively [9,41]. Compared with Fig. 4 (c), it can be seen that after hydrothermal aging, the proportion of CuO species in the catalysts with various Cu contents increased, while the proportion of Cu^{2+} species decreased. Consequently, the $\text{NH}_3\text{-SCR}$ catalytic activity

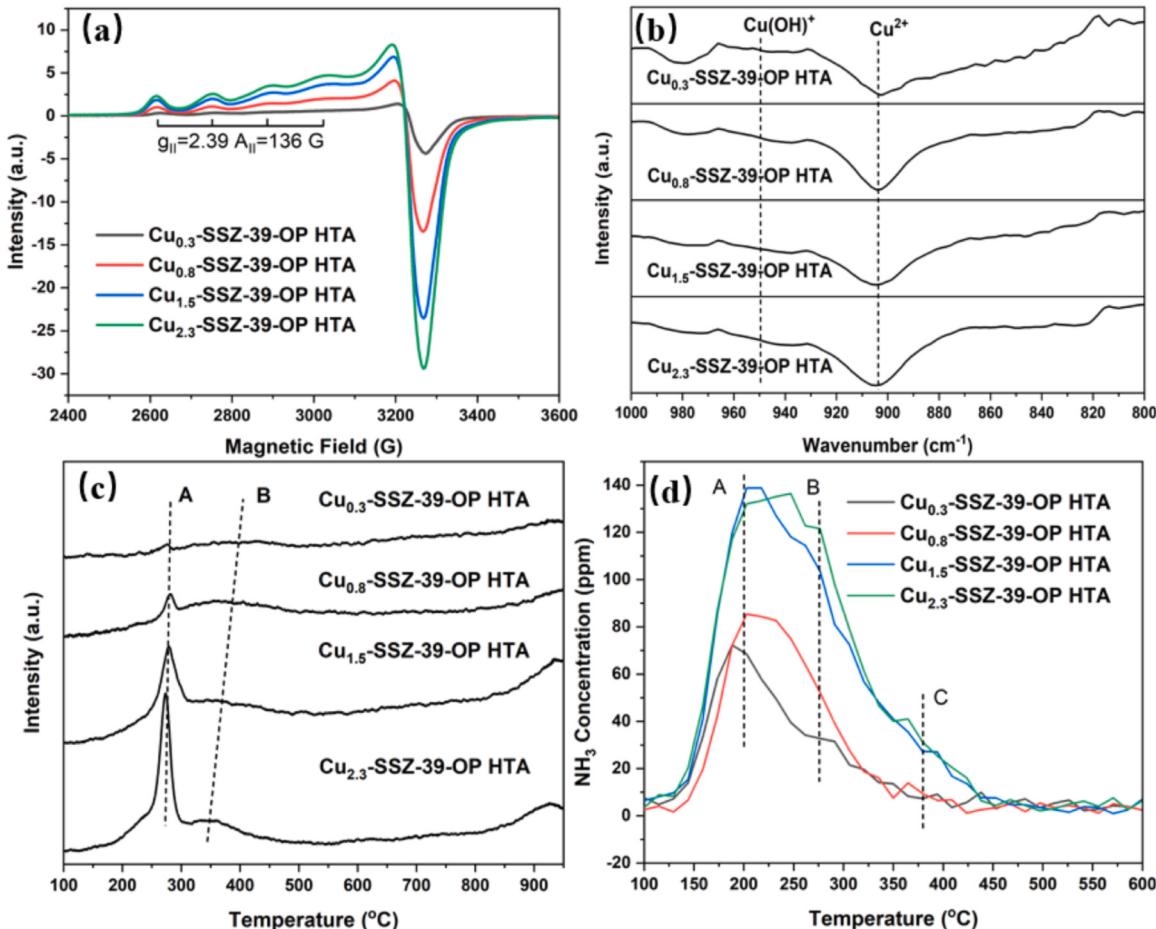


Fig. 7. (a) EPR spectra, (b) *in situ* DRIFTS of NH_3 adsorption spectra, (c) $\text{H}_2\text{-TPR}$ profiles and (d) $\text{NH}_3\text{-TPD}$ profiles of hydrothermally aged one-pot-synthesized Cu-SSZ-39 catalysts with various Cu contents.

of all hydrothermally aged one-pot-synthesized Cu-SSZ-39 catalysts decreased.

NH₃-TPD was used to characterize the changes in acid sites after hydrothermal aging, and the results are shown in Fig. 7 (d). In comparison with the fresh samples, both strong acid sites and weak acid sites in the hydrothermally aged catalysts decreased in quantity, while the number of weak acid sites slightly increased regardless of Cu content. According to the characterization of Cu species, we know that the quantity of Cu²⁺ decreased in the catalysts after hydrothermal aging, which can lead to a reduction in the number of moderate acid sites (Lewis acid sites). All one-pot-synthesized Cu-SSZ-39 catalysts faced dealumination after hydrothermal aging according to the NMR results; thus, the amount of strong acid sites (Brønsted acid sites) decreased. Meanwhile, dealumination also led to the generation of some terminal hydroxyl species, which led to increasing numbers of weak acid sites. Lewis acid sites acted as the main active centers, therefore, the loss of Lewis acid sites caused the decline of NH₃-SCR activity. Meanwhile, Brønsted acid sites facilitated the migration of Cu ions which was beneficial for NO_x conversion [50]. Therefore, the loss of Lewis acid sites and Brønsted acid sites caused the decline of NH₃-SCR activity as presented in Fig. 5.

3.2.2. SO₂ resistance of one-pot-synthesized Cu-SSZ-39 catalysts

Furthermore, Cu_{2.3}-SSZ-39-OP was chosen for sulfidation treatment. In order to compare it with the Cu-SSZ-39 catalyst prepared using the ion-exchange method, we chose a catalyst with the same Cu/Al ratio prepared using ZSM-5 as precursor. The elemental composition data for Cu_{2.3}-SSZ-39-OP and Cu_{2.0}-SSZ-39-IE are presented in Table 2. Due to the lower Si/Al ratio in Cu_{2.3}-SSZ-39-OP compared with Cu_{2.0}-SSZ-39-IE, the Cu content was slightly higher in Cu_{2.3}-SSZ-39-OP.

In our previous study, we found that the most deactivation of the Cu-SSZ-39 catalysts was obtained with the sulfation temperature at 400 °C. Moreover, the formation of CuSO₄ species was the main reason for the catalytic loss of the sulfated Cu-SSZ-39 catalysts [50]. To investigate the SO₂ resistance of Cu_{2.3}-SSZ-39-OP and Cu_{2.0}-SSZ-39-IE, the sulfation temperature was set as 400 °C. Furthermore, the regeneration temperature was set at 800 °C to get rid of CuSO₄ species.

As shown in Fig. 8, Cu_{2.3}-SSZ-39-OP and Cu_{2.0}-SSZ-39-IE exhibited comparable NH₃-SCR activity performance. Cu_{2.3}-SSZ-39-OP exhibited approximately 10 % higher NO_x conversion than Cu_{2.0}-SSZ-39-IE at 175°C; however, the difference in NO_x conversion was less than 3 % at other temperatures. Moreover, Cu_{2.0}-SSZ-39-IE outperformed Cu_{2.3}-SSZ-39-OP at 550°C, possibly due to the presence of CuO species in Cu_{2.3}-SSZ-39-OP.

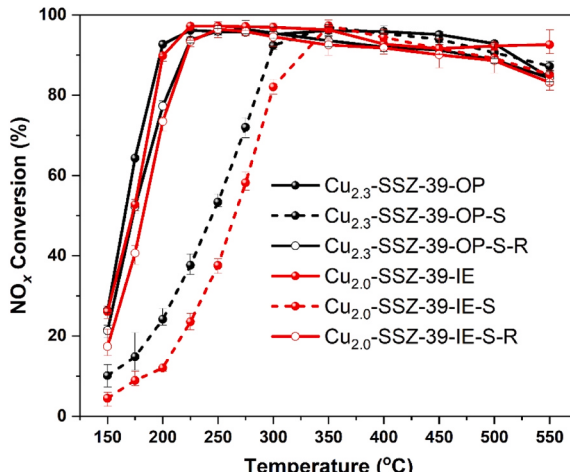


Fig. 8. NH₃-SCR activity of one-pot-synthesized Cu-SSZ-39 and ion-exchanged Cu-SSZ-39 after sulfidation and regeneration treatments.

After sulfidation treatment, Cu_{2.3}-SSZ-39-OP-S exhibited significantly better performance than Cu_{2.0}-SSZ-39-IE-S below 300°C. Cu_{2.3}-SSZ-39-OP-S exhibited over 10 % higher NO_x conversion than Cu_{2.0}-SSZ-39-IE-S in the temperature range of 200–300°C. After regeneration at 800°C for 2 h, both samples presented a substantial recovery of activity. Cu_{2.3}-SSZ-39-OP-S-R maintained higher catalytic activity than Cu_{2.0}-SSZ-39-IE-S-R between 150 and 200°C, and both catalysts achieved NO_x conversion over 90 % in the temperature range of 225–450°C. It is worth mentioning that Cu_{2.0}-SSZ-39-OP-S exhibited higher NO_x conversion at 550°C compared with its fresh state, which indicated non-selective oxidation of NH₃ was suppressed in Cu_{2.0}-SSZ-39-OP-S.

To further investigate the changes in Cu species during the sulfidation process, EPR experiments were conducted. As can be seen in Figure S5 (a), except for Cu_{2.0}-SSZ-39-IE-S, all other catalysts exhibited a fourfold hyperfine splitting pattern with $g_{\text{II}}=2.39$ and $A_{\text{II}}=134$ G. This confirmed that Cu species in these catalysts mainly existed in the form of Cu²⁺. Figure S5(b) presents the EPR signals of Cu_{2.0}-SSZ-39-IE-S and CuSO₄, and it appears that the EPR signal of Cu_{2.0}-SSZ-39-IE-S is a superposition of those of divalent Cu ions in zeolite and CuSO₄. This indicates the presence of a significant amount of CuSO₄ in Cu_{2.0}-SSZ-39-IE-S.

Subsequently, we summarized the relative Cu content of catalysts derived from EPR data, and results are shown in Figure S6. It can be seen that though Cu_{2.3}-SSZ-39-OP possessed higher Cu content than Cu_{2.0}-SSZ-39-IE, the amount of Cu²⁺ species was higher in Cu_{2.0}-SSZ-39-IE. This is due to the presence of a substantial amount of CuO in Cu_{2.3}-SSZ-39-OP. After sulfidation, Cu_{2.3}-SSZ-39-OP-S possessed more divalent Cu ions than Cu_{2.3}-SSZ-39-OP. This is because some of the CuO species were transformed into CuSO₄, as indicated by the increase in NO_x conversion at 550°C for Cu_{2.3}-SSZ-39-OP-S. In contrast, Cu_{2.0}-SSZ-39-IE-S had fewer divalent Cu ions than Cu_{2.0}-SSZ-39-IE, indicating that some Cu²⁺ species converted into CuO species. After regeneration, the amount of divalent Cu ions in Cu_{2.3}-SSZ-39-OP-S-R decreased, which indicated the decomposition of some CuSO₄ into CuO, accompanying with the decrease of NO_x conversion over 350 °C. Meanwhile, the quantity of divalent Cu ions further decreased in Cu_{2.0}-SSZ-39-IE-S-R, leading to a decrease in NO_x conversion at 550°C compared with its fresh state.

SO₂-TPD was conducted to distinguish the sulfated species in the Cu-SSZ-39 catalysts after sulfidation. The desorption of SO₂ around 400–550°C was due to H₂SO₄ species, and the peaks of SO₂ around 550–900°C were attributed to CuSO₄ species; meanwhile, Al₂(SO₄)₃ species decomposed over 900°C [50,51]. As can be seen in Figure S7, more H₂SO₄ species formed on Cu_{2.0}-SSZ-39-IE-S, and more CuSO₄ species formed on Cu_{2.3}-SSZ-39-OP-S. According to our previous study, H₂SO₄ species significantly affect low-temperature NO_x conversion due to the formation of (NH₄)₂SO₄ during SCR tests. Meanwhile, the formation of CuSO₄ species also led to a loss of catalytic activity due to the poisoning of Cu²⁺ species [50]. CuO species acted as sacrificial sites in Cu_{2.3}-SSZ-39-OP-S: they not only protected Cu²⁺ species, but also resulted in less formation of H₂SO₄ species. Therefore, Cu_{2.3}-SSZ-39-OP-S performed better than Cu_{2.0}-SSZ-39-IE-S in NH₃-SCR testing.

4. Discussion

Xiao et al. developed a one-pot synthesis of Cu-SSZ-13 using Cu-TEPA as an organic structure directing agent (OSDA) [34,52]. However, due to the excessive amounts of Cu species, after-treatment processes were necessary to obtain Cu-SSZ-13 with good NH₃-SCR performance [53–55]. Afterwards, Corma et al. used N,N, N-trimethyl-1-adamant ammonium and Cu-TEPA as co-templates to synthesize Cu-SSZ-13, which realized the control of Cu content without after-treatment processes. However, the NH₃-SCR catalytic activity of the one-pot-synthesized Cu-SSZ-13 was still not ideal, probably due to the presence of abundant Na⁺ and CuO species [18]. Subsequently, the one-pot synthesis of Cu-SSZ-39 catalysts was also realized by Corma et al., using USY as the precursor together with N, N-dimethyl-3,

5-dimethylpiperidinium and Cu-TEPA as co-templates. However, over 90 % NO_x conversion could be obtained only in the temperature range of 250–450°C, and neither the hydrothermal stability nor SO_2 resistance was evaluated [14].

One of the drawbacks of one-pot-synthesized Cu based zeolites is the presence of significant amounts of Na^+ in the product. Excessive Na^+ ions at ion-exchange sites occupy the location of Cu ions; therefore, the formation of CuO species is inevitable. Thus, both one-pot-synthesized Cu-SSZ-13 catalysts and Cu-SSZ-39 catalysts reported in the literature faced a significant decrease in NO_x conversion in the high-temperature range [14,18]. Recently, we found that the Cu-SSZ-39 catalysts obtained using ZSM-5 as precursor possessed excellent NH_3 -SCR activity and hydrothermal stability, which was attributed to their large particle size and excellent framework stability [17]. Therefore, we modified the one-pot synthesis of Cu-SSZ-39 catalysts using ZSM-5 as precursor, with the expectation of mitigating the negative impact of Na^+ ions. Moreover, in our study of the one-pot synthesis of Cu-SSZ-50 catalysts, we observed that increasing the amount of Cu-TEPA added led to a rise in the Si/Al ratio in products. A lower Si/Al ratio creates more ion-exchange sites for Cu ions, which can also mitigate the negative impact of Na^+ ions. [19]. Therefore, we also adjusted the amount of Cu-TEPA added to the starting gel. It turned out that $\text{Cu}_{1.5}\text{-SSZ-39-OP}$ and $\text{Cu}_{2.3}\text{-SSZ-39-OP}$ possessed lower Si/Al ratios, thus more Cu ions could be accommodated.

As illustrated in Fig. 5, one-pot-synthesized Cu-SSZ-39 catalysts, especially $\text{Cu}_{2.3}\text{-SSZ-39-OP}$, exhibited excellent NH_3 -SCR activity and hydrothermal stability. Over 90 % NO_x conversion was obtained between 200°C and 500°C for fresh $\text{Cu}_{2.3}\text{-SSZ-39-OP}$; meanwhile, hydrothermally aged $\text{Cu}_{2.3}\text{-SSZ-39-OP-HTA}$ possessed over 88 % NO_x conversion in the temperature range 225–500°C. To better illustrate the excellent catalytic performance of the one-pot-synthesized Cu-SSZ-39 catalyst, a table of the catalytic activity and hydrothermal stability of other reported zeolite catalysts was listed. As can be seen in Table 3, the catalytic activity of $\text{Cu}_{2.3}\text{-SSZ-39-OP}$ is comparable to those of the reported catalysts, except for Cu-SSZ-13 with the Cu content of 3.8 wt%, and Si/Al of 5.1 [55]. However, the hydrothermal stability of Cu-SSZ-13 (Cu: 3.8 wt%, Si/Al=5.1) was not as good as Cu-SSZ-39-OP. Meanwhile, Cu-LTA possessed the best hydrothermal stability that can stand 900 °C of hydrothermal treatment for 12 h [56]. However, its NO_x conversion at low-temperatures was lower than Cu-SSZ-39-OP even evaluated at a lower GHSV. In order to compare the performance of the one-pot-synthesized Cu-SSZ-39 catalyst with other catalyst under the same test condition, we chose a commercial Cu-SSZ-13 catalyst for additional activity comparison. The elemental composition of Cu-SSZ-13-commercial is shown in Table 2, with Si/Al ratio, Cu content and Cu/Al ratio similar to Cu-SSZ-39-OP. As presented in Figure S8,

the catalytic activity of Cu-SSZ-13-commercial in the fresh state was slightly better than $\text{Cu}_{2.3}\text{-SSZ-39-OP}$ below 175°C and above 500°C. Meanwhile, in the temperature range 225–400°C, $\text{Cu}_{2.3}\text{-SSZ-39-OP}$ exhibited better catalytic activity than Cu-SSZ-13-commercial. Moreover, it should be noted that the catalytic activity of $\text{Cu}_{2.3}\text{-SSZ-39-OP-HTA}$ was significantly better than that of Cu-SSZ-13-commercial-HTA after hydrothermal aging at 850°C for 16 h. This indicated that the one-pot-synthesized Cu-SSZ-39 catalysts developed in this study exhibited catalytic performance superior to that of commercial catalysts, and can meet the requirements for SCR catalysts in practical applications.

Despite trying to provide more ion-exchange sites for Cu ions by reducing the Si/Al ratio, formation of CuO was still inevitable in one-pot-synthesized Cu-SSZ-39 catalysts. In our previous study, we found that CuO in KFI zeolites transformed into CuSO_4 during the sulfidation process, leading to improvement in the high-temperature catalytic activity [60]. In this study, we also discovered that CuO species worked as sacrificial sites under sulfidation in one-pot-synthesized Cu-SSZ-39 catalysts. The function of different Cu species of the one-pot-synthesized Cu-SSZ-39 catalysts without and with SO_2 during NH_3 -SCR process was illustrated in the Scheme 1. During the NH_3 -SCR process, Cu^{2+} species acted as the main active sites for NO_x conversion. When SO_2 existed, CuO species can act as sacrificial sites, therefore Cu^{2+} species are protected. Based on this, we propose a strategy to enhance the sulfur resistance of Cu-based zeolites by generating CuO species. First and foremost, it is crucial to ensure that the CuO species in the catalyst do not have a significant negative impact on the NH_3 -SCR activity and hydrothermal stability of the zeolite catalysts. Additionally, CuO species should be easily exposed to SO_2 , and work as sacrificial sites. One-pot-synthesized Cu-SSZ-39 zeolite seems to be an ideal candidate with these characteristics. Cu species were well dispersed in the one-pot-synthesized Cu-SSZ-39 catalysts, and the formation of CuO species did not affect the NH_3 -SCR activity or hydrothermal stability. As a result, one-pot-synthesized Cu-SSZ-39 catalysts not only exhibited excellent activity and hydrothermal stability, but also possessed remarkable sulfur resistance. Furthermore, we also proposed a regeneration condition to recycle the SO_2 poisoned catalyst. After being treated at 800°C for 2 h under 10 % $\text{H}_2\text{O}/\text{air}$, most of the catalytic activity can be recovered. Therefore, the one-pot-synthesized Cu-SSZ-39 catalysts possess bright prospect of application.

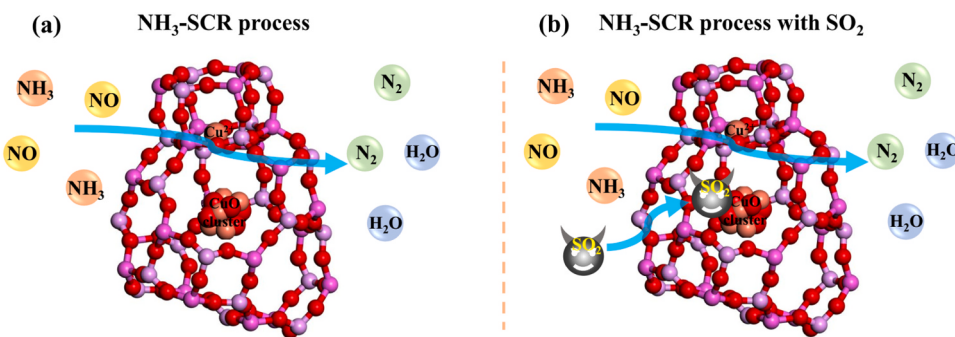
5. Conclusion

Supported by theoretical calculations, this study developed a facile one-pot synthesis method for Cu-SSZ-39 zeolites. The addition of Cu-

Table 3

The NH_3 -SCR catalytic activity and hydrothermal stability of the one-pot-synthesized Cu-SSZ-39 catalysts and the other reported catalysts.

Catalysts	NO_x conversion (fresh)	NO_x conversion (aged)	Test condition	Hydrothermal condition	Reference
Cu-SSZ-13 (Cu: 3.8 wt%, Si/Al=5.1)	200–550 °C: >95 %	225–450 °C: >90 %	$[\text{NO}] = [\text{NH}_3] = 500 \text{ ppm}$, $[\text{O}_2] = [\text{H}_2\text{O}] = 5\%$, GHSV= 400,000 h^{-1}	10 % $\text{H}_2\text{O}/\text{air}$, 800 °C, 16 h	[55]
Cu-SSZ-13 (Cu: 4.1 wt%, Si/Al=6)	250–550 °C: >90 %	250–450 °C: >85 %	$[\text{NO}] = [\text{NH}_3] = 500 \text{ ppm}$, $[\text{O}_2] = [\text{H}_2\text{O}] = 10\%$, GHSV= 240,000 h^{-1}	10 % H_2O , 10 % O_2 , 750 °C, 16 h	[57]
Cu-SSZ-13 (Cu:2.92 wt%, Si/Al=14)	200–400 °C: >95 %	240–390 °C: >90 %	$[\text{NO}] = [\text{NH}_3] = 500 \text{ ppm}$, $[\text{O}_2] = 5\%$, $[\text{H}_2\text{O}] = 10\%$, GHSV= 100,000 h^{-1}	10 % $\text{H}_2\text{O}/\text{air}$, 750 °C, 24 h	[37]
Cu-SSZ-39 (Cu:3.4 wt%, Si/Al=6.5)	225–550 °C: >90 %	250–400 °C: >85 %	$[\text{NO}] = [\text{NH}_3] = 500 \text{ ppm}$, $[\text{O}_2] = [\text{H}_2\text{O}] = 5\%$, GHSV= 250,000 h^{-1}	10 % $\text{H}_2\text{O}/\text{air}$, 850 °C, 16 h	[9]
Cu-KFI (Cu:2.8 wt%, Si/Al~5)	200–550 °C: >90 %	250–450 °C: >90 %	$[\text{NO}] = [\text{NH}_3] = 500 \text{ ppm}$, $[\text{O}_2] = [\text{H}_2\text{O}] = 5\%$, GHSV= 80,000 h^{-1}	10 % $\text{H}_2\text{O}/\text{air}$, 800 °C, 16 h	[58]
Cu-SSZ-16 (Cu:2.93 wt%, Si/Al=6.7)	225–400 °C: >90 %	225–400 °C: >85 %	$[\text{NO}] = [\text{NH}_3] = 500 \text{ ppm}$, $[\text{O}_2] = [\text{H}_2\text{O}] = 5\%$, GHSV= 200,000 h^{-1}	10 % $\text{H}_2\text{O}/\text{air}$, 800 °C, 16 h	[59]
Cu-LTA (Cu:3.2 wt%, Si/Al=16)	225–550 °C: >90 %	250–550 °C: >80 %	$[\text{NO}] = [\text{NH}_3] = 500 \text{ ppm}$, $[\text{O}_2] = 5\%$, $[\text{H}_2\text{O}] = 10\%$, GHSV= 100,000 h^{-1}	10 % $\text{H}_2\text{O}/\text{air}$, 900 °C, 12 h	[56]
Cu-SSZ-50 (Cu: 3.2 wt%, Si/Al=7.7)	200–450 °C: >90 %	250–450 °C: >80 %	$[\text{NO}] = [\text{NH}_3] = 500 \text{ ppm}$, $[\text{O}_2] = [\text{H}_2\text{O}] = 5\%$, GHSV= 200,000 h^{-1}	10 % $\text{H}_2\text{O}/\text{air}$, 750 °C, 16 h	[19]
Cu-SSZ-39 (Cu:2.3 wt%, Si/Al=6.6)	200–500 °C: >90 %	225–500 °C: >85 %	$[\text{NO}] = [\text{NH}_3] = 500 \text{ ppm}$, $[\text{O}_2] = [\text{H}_2\text{O}] = 5\%$, GHSV= 200,000 h^{-1}	10 % $\text{H}_2\text{O}/\text{air}$, 850 °C, 16 h	This study



Scheme 1. Mechanism diagram of the roles of Cu^{2+} and CuO species in the (a) NH_3 -SCR reaction process; (b) NH_3 -SCR reaction process with SO_2 .

TEPA did not affect the transformation process of ZSM-5 to Cu-SSZ-39. However, an excess of Cu-TEPA can influence the Si/Al ratio of Cu-SSZ-39 catalysts and the formation of CuO species. Despite the presence of CuO , the one-pot-synthesized Cu-SSZ-39 sample exhibited superior hydrothermal stability compared with commercial Cu-SSZ-13 catalysts. Simultaneously, the presence of CuO played a protective role during sulfurization, enhancing the resistance to sulfur for the one-pot-synthesized Cu-SSZ-39 compared with conventionally ion-exchanged samples. Considering the facile synthesis process and excellent catalytic performance, one-pot-synthesized Cu-SSZ-39 catalysts hold great promise for practical applications.

CRediT authorship contribution statement

Jinpeng Du: Writing – original draft, Methodology, Investigation, Data curation, Conceptualization. **Xiaomin Tang:** Methodology, Investigation. **Chi Huang:** Investigation. **Jianqi Liu:** Investigation. **Yulong Shan:** Writing – review & editing, Investigation, Formal analysis, Conceptualization. **Yan Zhang:** Formal analysis, Conceptualization. **Mingsong Ren:** Investigation. **Yinhuan Wang:** Investigation. **Wenpo Shan:** Supervision, Conceptualization. **Yunbo Yu:** Supervision, Conceptualization. **Anmin Zheng:** Writing – review & editing, Supervision. **Hong He:** Writing – review & editing, Supervision, Resources, Project administration.

Declaration of Competing Interest

The authors declare that they have no known competing financial interests or personal relationships that could have appeared to influence the work reported in this paper.

Data availability

Data will be made available on request.

Acknowledgements

This work was financially supported by the National Natural Science Foundation of China (52200136, 52270112, 22202215, 52225004). The National Key R&D Program of China (2022YFC3704400), National Energy-Saving and Low-Carbon Materials Production and Application Demonstration Platform Program (TC220H06N).

Appendix A. Supporting information

Details for catalyst preparation process and characterization. SEM images of one-pot-synthesized Cu-SSZ-39 catalysts with different crystallization times, TEM and EDS-mapping images of the one-pot-synthesized Cu-SSZ-39 catalysts. N_2O concentration of the catalysts during NH_3 -SCR tests. Relative Cu content of fresh and hydrothermally aged one-pot-synthesized Cu-SSZ-39 catalysts according to EPR results.

EPR spectra of catalysts after sulfidation and regeneration experiments. Relative Cu content of one-pot-synthesized Cu-SSZ-39 and ion-exchanged Cu-SSZ-39 catalysts according to EPR results. SO_2 -TPD profiles of Cu-SSZ-39 catalysts. NH_3 -SCR performance of $\text{Cu}_{2.3}\text{-SSZ-39-OP}$ and commercial Cu-SSZ-13 catalyst.

References

- [1] D. Ding, J. Xing, S. Wang, Z. Dong, F. Zhang, S. Liu, J. Hao, Optimization of a NO_x and VOC cooperative control strategy based on clean air benefits, Environ. Sci. Technol. 56 (2022) 739–749.
- [2] Y. Tan, P. Henderick, S. Yoon, J. Herner, T. Montes, K. Boriboonsomsin, K. Johnson, G. Scora, D. Sandez, T.D. Durbin, On-board sensor-based NO_x emissions from heavy-duty diesel vehicles, Environ. Sci. Technol. 53 (2019) 5504–5511.
- [3] G.A. Bishop, M.J. Haugen, B.C. McDonald, A.M. Boies, Utah wintertime measurements of heavy-duty vehicle nitrogen oxide emission factors, Environ. Sci. Technol. 56 (2022) 1885–1893.
- [4] H. Kong, J. Lin, L. Chen, Y. Zhang, Y. Yan, M. Liu, R. Ni, Z. Liu, H. Weng, Considerable unaccounted local sources of NO_x emissions in China revealed from satellite, Environ. Sci. Technol. 56 (2022) 7131–7142.
- [5] S. Jiang, T. Li, J. Zheng, H. Zhang, X. Li, T. Zhu, Unveiling the remarkable arsenic resistance origin of alumina promoted cerium-tungsten catalysts for NH_3 -SCR, Environ. Sci. Technol. 54 (2020) 14740–14749.
- [6] P. Li, Y. Xin, Q. Li, Z. Wang, Z. Zhang, L. Zheng, Ce-Ti amorphous oxides for selective catalytic reduction of NO with NH_3 : confirmation of Ce-O-Ti active sites, Environ. Sci. Technol. 46 (2012) 9600–9605.
- [7] Q. Lin, S. Xu, H. Zhao, S. Liu, H. Xu, Y. Dan, Y. Chen, Highlights on key roles of Y on the hydrothermal stability at 900 °C of Cu/SSZ-39 for NH_3 -SCR, ACS Catal. 12 (2022) 14026–14039.
- [8] G. Sun, R. Yu, L. Xu, B. Wang, W. Zhang, Enhanced hydrothermal stability and SO_2 -tolerance of Cu-Fe modified AEI zeolite catalysts in NH_3 -SCR of NO_x , Catal. Sci. Technol. 12 (2022) 3898–3911.
- [9] Y. Shan, W. Shan, X. Shi, J. Du, Y. Yu, H. He, A comparative study of the activity and hydrothermal stability of Al-rich Cu-SSZ-39 and Cu-SSZ-13, Appl. Catal. B Environ. 264 (2020) 118511–118520.
- [10] J.E. Schmidt, R. Oord, W. Guo, J.D. Poplawsky, B.M. Weckhuysen, Nanoscale tomography reveals the deactivation of automotive copper-exchanged zeolite catalysts, Nat. Commun. 8 (2017) 1666.
- [11] K. Xie, K. Leistner, K. Wijayanti, A. Kumar, K. Kamasamudram, L. Olsson, Influence of phosphorus on Cu-SSZ-13 for selective catalytic reduction of NO_x by ammonia, Catal. Today 297 (2017) 46–52.
- [12] I. Heo, S. Sung, M.B. Park, T.S. Chang, Y.J. Kim, B.K. Cho, S.B. Hong, J.W. Choung, I.-S. Nam, Effect of Hydrocarbon on DeNO_x Performance of selective catalytic reduction by a combined reductant over Cu-containing zeolite catalysts, ACS Catal. 9 (2019) 9800–9812.
- [13] M. Moliner, C. Franch, E. Palomares, M. Grill, A. Corma, Cu-SSZ-39, an active and hydrothermally stable catalyst for the selective catalytic reduction of NO_x , Chem. Commun. (Camb.) 48 (2012) 8264–8266.
- [14] N. Martin, C.R. Boruntea, M. Moliner, A. Corma, Efficient synthesis of the Cu-SSZ-39 catalyst for DeNO_x applications, Chem. Commun. (Camb.) 51 (2015) 11030–11033.
- [15] H. Xu, W. Chen, Q. Wu, C. Lei, J. Zhang, S. Han, L. Zhang, Q. Zhu, X. Meng, D. Dai, S. Maurer, A.-N. Parvulescu, U. Müller, W. Zhang, T. Yokoi, X. Bao, B. Marler, D. E. De Vos, U. Kolb, A. Zheng, F.-S. Xiao, Transformation synthesis of aluminosilicate SSZ-39 zeolite from ZSM-5 and beta zeolite, J. Mater. Chem. A 7 (2019) 4420–4425.
- [16] H. Xu, J. Zhang, Q. Wu, W. Chen, C. Lei, Q. Zhu, S. Han, J. Fei, A. Zheng, L. Zhu, X. Meng, S. Maurer, D. Dai, A.N. Parvulescu, U. Muller, F.-S. Xiao, Direct synthesis of aluminosilicate SSZ-39 zeolite using colloidal silica as a starting source, ACS Appl. Mater. Interfaces 11 (2019) 23112–23117.
- [17] J. Du, S. Han, C. Huang, Y. Shan, Y. Zhang, W. Shan, H. He, Comparison of precursors for the synthesis of Cu-SSZ-39 zeolite catalysts for NH_3 -SCR reaction, Appl. Catal. B Environ. 338 (2023) 123072–123081.

- [18] R. Martínez-Franco, M. Moliner, J.R. Thogersen, A. Corma, Efficient one-pot preparation of Cu-SSZ-13 materials using cooperative OSDAs for their catalytic application in the SCR of NO_x , *ChemCatChem* 5 (2013) 3316–3323.
- [19] J. Du, J. Wang, Y. Shan, S. Han, W. Shan, H. He, Promoted NH₃-SCR activity and hydrothermal stability of Cu-SSZ-50 catalyst synthesized by one-pot method, *Chin. Chem. Lett.* (2023) 108781–108786 (CCLET).
- [20] J. Wang, D. Fan, T. Yu, J. Wang, T. Hao, X. Hu, M. Shen, W. Li, Improvement of low-temperature hydrothermal stability of Cu/SAPO-34 catalysts by Cu²⁺ species, *J. Catal.* 322 (2015) 84–90.
- [21] C. Fan, Z. Chen, L. Pang, S. Ming, X. Zhang, K.B. Albert, P. Liu, H. Chen, T. Li, The influence of Si/Al ratio on the catalytic property and hydrothermal stability of Cu-SSZ-13 catalysts for NH₃-SCR, *Appl. Catal. A Gen.* 550 (2018) 256–265.
- [22] J. Wang, L. Wang, D. Zhu, W. Cui, P. Tian, Z. Liu, One-pot synthesis of Na⁽⁺⁾-free Cu-SSZ-13 and its application in the NH₍₃₎-SCR reaction, *Chem. Commun. (Camb.)* 57 (2021) 4898–4901. (<http://www.iza-structure.org/databases/>).
- [24] A.K. Rappé, C.J. C, K.S. Colwell, W.A. Goddard III, W.M. S, UFF, a full periodic table force field for molecular mechanics and molecular dynamics simulations, *J. Am. Chem. Soc.* 114 (1992) 10024–10035.
- [25] J.D. Gale, A.L. Rohl, The General Utility Lattice Program (GULP), *Mol. Simul.* 29 (2003) 291–341.
- [26] Y. Ma, X. Tang, J. Hu, Y. Ma, W. Chen, Z. Liu, S. Han, C. Xu, Q. Wu, A. Zheng, L. Zhu, X. Meng, F.-S. Xiao, Design of a small organic template for the synthesis of self-pillared pentasil zeolite nanosheets, *J. Am. Chem. Soc.* 144 (2022) 6270–6277.
- [27] F. Daeyaert, F. Ye, M.W. Deem, Machine-learning approach to the design of OSDAs for zeolite beta, *P. Natl. Acad. Sci. USA* 116 (2019) 3413–3418.
- [28] J.E. Schmidt, D. Fu, M.W. Deem, B.M. Weckhuysen, Template-framework interactions in tetraethylammonium-directed zeolite synthesis, *Angew. Chem. Int. Ed.* 55 (2016) 16044–16048.
- [29] M. Gálvez-Llompart, J. Gálvez, F. Rey, G. Sastre, Identification of new templates for the synthesis of BEA, BEC, and ISV zeolites using molecular topology and Monte Carlo techniques, *J. Chem. Inf. Model.* 60 (2020) 2819–2829.
- [30] T. Sonoda, T. Maruo, Y. Yamasaki, N. Tsunooji, Y. Takamitsu, M. Sadakane, T. Sano, Synthesis of high-silica AEI zeolites with enhanced thermal stability by hydrothermal conversion of FAU zeolites, and their activity in the selective catalytic reduction of NO_x with NH₃, *J. Mater. Chem. A* 3 (2015) 857–865.
- [31] J. Du, Y. Shan, Y. Sun, M. Gao, Z. Liu, X. Shi, Y. Yu, H. He, Unexpected increase in low-temperature NH₃-SCR catalytic activity over Cu-SSZ-39 after hydrothermal aging, *Appl. Catal. B Environ.* 294 (2021) 120237–120246.
- [32] J. Zhang, Y. Chu, F. Deng, Z. Feng, X. Meng, F.-S. Xiao, Evolution of D6R units in the interzeolite transformation from FAU, MFI or *BEA into AEI: transfer or reassembly? *Inorg. Chem. Front.* 7 (2020) 2204–2211.
- [33] B. Ipek, M.J. Wulfers, H. Kim, F. Göltl, I. Hermans, J.P. Smith, K.S. Booksh, C. M. Brown, R.F. Lobo, Formation of [Cu₂O₂]²⁺ and [Cu₂O]²⁺ toward C–H Bond Activation in Cu-SSZ-13 and Cu-SSZ-39, *ACS Catal.* 7 (2017) 4291–4303.
- [34] L. Ren, Y. Zhang, S. Zeng, L. Zhu, Q. Sun, H. Zhang, C. Yang, X. Meng, X. Yang, F.-S. Xiao, Design and synthesis of a catalytically active Cu-SSZ-13 zeolite from a copper-amine complex template, *Chin. J. Catal.* 33 (2012) 92–105.
- [35] R. Li, Y. Zhu, Z. Zhang, C. Zhang, G. Fu, X. Yi, Q. Huang, F. Yang, W. Liang, A. Zheng, J. Jiang, Remarkable performance of selective catalytic reduction of NO_x by ammonia over copper-exchanged SSZ-52 catalysts, *Appl. Catal. B Environ.* 283 (2021) 119641–119650.
- [36] R. Osuga, T. Takeuchi, M. Sawada, Y. Kunitake, T. Matsumoto, S. Yasuda, H. Onozuka, S. Tsutsumi, J.N. Kondo, H. Gies, T. Yokoi, Fabrication of AEI-type aluminosilicate with sheet-like morphology for direct conversion of propene to butenes, *Catal. Sci. Technol.* 11 (2021) 5839–5848.
- [37] Y.J. Kim, J.K. Lee, K.M. Min, S.B. Hong, I.-S. Nam, B.K. Cho, Hydrothermal stability of CuSSZ13 for reducing NO_x by NH₃, *J. Catal.* 311 (2014) 447–457.
- [38] R. Li, X. Jiang, J. Lin, Z. Zhang, Q. Huang, G. Fu, Y. Zhu, J. Jiang, Understanding the influence of hydrothermal treatment on NH₃-SCR of NO activity over Cu-SSZ-16, *Chem. Eng. J.* 441 (2022) 136021–136030.
- [39] D. Wang, F. Gao, C.H.F. Peden, J. Li, K. Kamasamudram, W.S. Epling, Selective catalytic reduction of NO_x with NH₃ over a Cu-SSZ-13 catalyst prepared by a solid-state ion-exchange method, *ChemCatChem* 6 (2014) 1579–1583.
- [40] J. Luo, D. Wang, A. Kumar, J. Li, K. Kamasamudram, N. Currier, A. Yezers, Identification of two types of Cu sites in Cu/SSZ-13 and their unique responses to hydrothermal aging and sulfur poisoning, *Catal. Today* 267 (2016) 3–9.
- [41] S. Han, Q. Ye, S. Cheng, T. Kang, H. Dai, Effect of the hydrothermal aging temperature and Cu/Al ratio on the hydrothermal stability of CuSSZ-13 catalysts for NH₃-SCR, *Catal. Sci. Technol.* 7 (2017) 703–717.
- [42] H. Jiang, B. Guan, H. Lin, Z. Huang, Cu/SSZ-13 zeolites prepared by in situ hydrothermal synthesis method as NH₃-SCR catalysts: influence of the Si/Al ratio on the activity and hydrothermal properties, *Fuel* 255 (2019) 115587–115603.
- [43] J. Liang, Y. Mi, G. Song, H. Peng, Y. Li, R. Yan, W. Liu, Z. Wang, P. Wu, F. Liu, Environmental benign synthesis of nano-SSZ-13 via FAU trans-crystallization: enhanced NH₃-SCR performance on Cu-SSZ-13 with nano-size effect, *J. Haz. Mat.* 398 (2020) 122986–122997.
- [44] H. Tian, Y. Ping, Y. Zhang, Z. Zhang, L. Sun, P. Liu, J. Zhu, X. Yang, Atomic layer deposition of silica to improve the high-temperature hydrothermal stability of Cu-SSZ-13 for NH₃ SCR of NO_x, *J. Haz. Mat.* 416 (2021) 126194–126203.
- [45] D. Yao, B. Liu, F. Wu, Y. Li, X. Hu, W. Jin, X. Wang, N₂O formation mechanism during low-temperature NH₃-SCR over Cu-SSZ-13 catalysts with different Cu loadings, *Ind. Eng. Chem. Res.* 60 (28) (2021) 10083–10093.
- [46] B. Liu, D. Yao, F. Wu, L. Wei, X. Li, X. Wang, Experimental investigation on N₂O formation during the selective catalytic reduction of NO_x with NH₃ over Cu-SSZ-13, *Ind. Eng. Chem. Res.* 58 (45) (2019) 20516–20527.
- [47] X. Yong, C. Zhang, M. Wei, P. Xie, Y. Li, Promotion of the performance of Cu-SSZ-13 for selective catalytic reduction of NO_x by ammonia in the presence of SO₂ during high temperature hydrothermal aging, *J. Catal.* 394 (2021) 228–235.
- [48] J. Zhu, Z. Liu, L. Xu, T. Ohnishi, Y. Yanaba, M. Ogura, T. Wakihara, T. Okubo, Understanding the high hydrothermal stability and NH₃-SCR activity of the fast-synthesized ERI zeolite, *J. Catal.* 391 (2020) 346–356.
- [49] T. Zhang, F. Qiu, J. Li, Design and synthesis of core-shell structured meso -Cu-SSZ-13@mesoporous aluminosilicate catalyst for SCR of NO_x with NH₃: Enhancement of activity, hydrothermal stability and propene poisoning resistance, *Appl. Catal. B Environ.* 195 (2016) 48–58.
- [50] J. Du, Y. Shan, G. Xu, Y. Sun, Y. Wang, Y. Yu, W. Shan, H. He, Effects of SO₂ on Cu-SSZ-39 catalyst for the selective catalytic reduction of NO_x with NH₃, *Catal. Sci. Technol.* 10 (2020) 1256–1263.
- [51] W. Su, Z. Li, Y. Zhang, C. Meng, J. Li, Identification of sulfate species and their influence on SCR performance of Cu/CHA catalyst, *Catal. Sci. Technol.* 7 (7) (2017) 1523–1528.
- [52] L. Ren, L. Zhu, C. Yang, Y. Chen, Q. Sun, H. Zhang, C. Li, F. Nawaz, X. Meng, F.-S. Xiao, Designed copper-amine complex as an efficient template for one-pot synthesis of Cu-SSZ-13 zeolite with excellent activity for selective catalytic reduction of NO_x by NH₃, *Chem. Commun. (Camb.)* 47 (35) (2011) 9789–9791.
- [53] L. Xie, F. Liu, L. Ren, X. Shi, F.-S. Xiao, H. He, Excellent performance of one-pot synthesized Cu-SSZ-13 catalyst for the selective catalytic reduction of NO_x with NH₃, *Environ. Sci. Technol.* 48 (2014) 566–572.
- [54] L. Xie, F. Liu, X. Shi, F.-S. Xiao, H. He, Effects of post-treatment method and Na co-cation on the hydrothermal stability of Cu-SSZ-13 catalyst for the selective catalytic reduction of NO_x with NH₃, *Appl. Catal. B Environ.* 179 (2015) 206–212.
- [55] Y. Shan, J. Du, Y. Yu, W. Shan, X. Shi, H. He, Precise control of post-treatment significantly increases hydrothermal stability of in-situ synthesized Cu-zeolites for NH₃-SCR reaction, *Appl. Catal. B Environ.* 266 (2020) 118655–118666.
- [56] T. Ryu, N.H. Ahn, S. Seo, J. Cho, H. Kim, D. Jo, G.T. Park, P.S. Kim, C.H. Kim, E. L. Bruce, P.A. Wright, I.S. Nam, S.B. Hong, Fully copper-exchanged high-silica LTA zeolites as unrivaled hydrothermally stable NH₃-SCR catalysts, *Angew. Chem. Int. Ed. Engl.* 56 (12) (2017) 3256–3260.
- [57] D. Wang, Y. Jangjou, Y. Liu, M.K. Sharma, J. Luo, J. Li, K. Kamasamudram, W. S. Epling, A comparison of hydrothermal aging effects on NH₃-SCR of NO_x over Cu-SSZ-13 and Cu-SAPO-34 catalysts, *Appl. Catal. B Environ.* 165 (2015) 438–445.
- [58] S. Han, X. Tang, L. Wang, Y. Ma, W. Chen, Q. Wu, L. Zhang, Q. Zhu, X. Meng, A. Zheng, F. Xiao, Potassium-directed sustainable synthesis of new high silica small-pore zeolite with KFI structure (ZJM-7) as an efficient catalyst for NH₃-SCR reaction, *Appl. Catal. B Environ.* 281 (2021) 119480–119487.
- [59] S. Han, W. Rao, J. Hu, X. Tang, Y. Ma, J. Du, Z. Liu, Q. Wu, Y. Ma, X. Meng, W. Shan, F.-S. Xiao, H. He, Direct synthesis of high silica SSZ-16 zeolite with extraordinarily superior performance in NH₃-SCR reaction, *Appl. Catal. B Environ.* 322 (2023) 122746–122753.
- [60] Z. Liu, Y. Shan, S. Han, Y. Fu, J. Du, Y. Sun, X. Shi, Y. Yu, H. He, Insights into SO₂ poisoning mechanisms of fresh and hydrothermally aged Cu-KFI catalysts for NH₍₃₎-SCR reaction, *Environ. Sci. Technol.* 57 (2023) 4308–4317.